EarthArXiv Coversheet

Authors

John G. Ruck[1], **Cristina G. Wilson**[2], **Thomas Shipley**[3], **Daniel Koditschek**[4], **Feifei Qian**[5], **Douglas Jerolmack**[1,6]

Affiliations

[1]University of Pennsylvania, Earth and Environmental Science, [2]Oregon State University, Collaborative Robotics and Intelligent Systems Institute, [3]Temple University, Psychology, [4]University of Pennsylvania, Electrical and Systems Engineering, [5]University of Southern California, Electrical Engineering, [6]University of Pennsylvania, Mechanical Engineering and Applied Mechanics

Email

Corresponding author: sediment@sas.upenn.edu

Peer-review statement

This manuscript is in second-round review at *Geophysical Research Letters* and has been peer-reviewed once.

Downslope weakening of soil revealed by a rapid robotic rheometer

John G. Ruck[1], Cristina G. Wilson[2], Thomas Shipley[3], Daniel Koditschek[4], Feifei Qian[5], Douglas Jerolmack[1,6]

[1]University of Pennsylvania, Earth and Environmental Science
[2]Oregon State University, Collaborative Robotics and Intelligent Systems Institute
[3]Temple University, Psychology
[4]University of Pennsylvania, Electrical and Systems Engineering
[5]University of Southern California, Electrical Engineering
[6]University of Pennsylvania, Mechanical Engineering and Applied Mechanics

Key Points:

- Soil strength controls hillslope stability and erosion, but is difficult to measure
- A novel robotic soil rheometer reveals downslope soil weakening
- Weakening results from increasing porosity associated with soil weathering

Corresponding author: Douglas Jerolmack, `sediment@sas.upenn.edu`

Abstract

Moving down a hillslope from ridge to valley, soil develops and becomes increasingly weathered. Downslope variation in clay content, organic matter, and porosity should produce concomitant changes in soil strength that influence slope stability and erosion. This has yet to be demonstrated, however, because *in-situ* measurements of soil rheology are challenging and rare. Here we employ a robotic leg as a mechanically sensitive and time-efficient penetrometer to map soil strength along a canonical temperate hillslope profile. We observe a systematic downslope weakening, and increasing heterogeneity, of soil strength associated with a transition from sand-rich ridge materials to cohesive valley bottom soil aggregates. Weathering-induced changes in soil composition lead to physically distinct mechanical behaviors in cohesive soils that depart from the behavior observed for sand. We also demonstrate the promise that legged robots may use their limbs to sense and improve mobility in complex environments, with implications for planetary exploration.

Plain Language Summary

Our infrastructure and livelihoods are literally built on soil. The strength of soil governs its stability under disturbance – with impacts on agriculture, ecosystems and natural hazards. Soil strength is very sensitive to variations in composition including clay, organic material, and water content. This means that strength must be directly measured in the field, but such measurements are rare because existing techniques are expensive, time consuming, and require specialized equipment. We develop a robotic soil strength tester that mimics intrusion behavior of plants and animals, and that allows rapid and reliable measurements. We use this device to demonstrate that soil gradually softens along a natural hillside, as it becomes progressively enriched with clay and organic matter downslope. Our device is based on a robot leg, and represents a significant step toward the development of legged robots that are capable of mapping soil strength by walking.

1 Introduction

In the canonical hillslope profile, exposed bedrock at the ridge disintegrates to form soil, that weathers as it creeps downslope over thousands of years (Ballantyne, 2009; Huggett, 2011). Along this gradient, soil is progressively enriched in clay and organic matter and is increasingly bioturbated (Wroth, 1984; Huggett, 2011), increasing soil cohesion and porosity (Famiglietti et al., 1998) with profound consequences for the infiltration and retention of water (Hawley et al., 1983). This downslope evolution in composition is expected to substantially change soil mechanical properties, and indeed several studies have observed differences in shear/compressive strength (Paaswell, 1973; Saravanan et al., 2020) and erodibility (Bryan, 2000; J.-L. Briaud et al., 2019) of soil as a result of variation in composition. There are, however, no systematic studies of downslope changes in soil strength that we know of. This is due in part to challenges in obtaining *in-situ* measurements; relatively time and cost efficient methods such as shear vanes or the standard penetration test are insufficiently sensitive and subject to user error (Mayne & Dumas, 1997), while mechanically sensitive geotechnical approaches like the cone penetration test (J. Briaud, 2013) are expensive, unwieldy, and require specialized equipment and training. What is needed is a technique for rapid and reliable *in-situ* measurements of soil mechanical properties. If this technique were sufficiently compact and robust, it could also find use in characterizing the regolith of other planetary surfaces like the Moon and Mars (Chhaniyara et al., 2012; Seweryn et al., 2014; Just et al., 2020).

Laboratory studies using sensitive intruders, on dry sand, have been able to resolve small changes in friction and explain them using theory (Brzinski III et al., 2013; Kang et al., 2018; Feng et al., 2019; Roth et al., 2021; Roth, 2021). There are two challenges

to extending these granular penetration findings to the field. First is that natural soils are compositionally more than sand; the addition of clay, organic matter, and water introduces cohesion that fundamentally alters soil structure across scales (Santamarina & Cho, 2004; Bronick & Lal, 2005; Richefeu et al., 2006; Diel et al., 2019; Vu et al., 2022). As a result, cohesive natural soils can exhibit a different force response to penetration (Janda & Ooi, 2016). The second challenge is how to take measurements of laboratory quality to a field setting, where the requirements outlined above prohibit unwieldy and expensive equipment. This challenge has recently been overcome by our team, where we demonstrated that a robotic leg – originally developed for locomotion of legged robots on challenging terrain – could be modified to be a sensitive and efficient field soil rheometer (Qian et al., 2019). Here we use this robotic rheometer to probe soil strength along a downslope weathering gradient in a forested, temperate hillslope in Philadelphia, PA, and validate our approach through controlled laboratory tests. We find that soils become weaker, and depart from the behavior of cohesionless sand, moving downslope from a sandy and relatively dry ridge soil toward a clay-rich and relatively moist valley bottom soil. We infer that the primary control on strength behavior is porosity; the aggregate-rich weathered soil is highly compactible. Because this leg can be mounted on a locomoting platform, this work opens the possibility of using legged robots to map soil strength across landscapes by walking.

2 Materials & Methods

2.1 Theoretical and phenomenological background

The vertical force measured on an intruder, F_z, increases monotonically with penetration depth, h (Stone et al., 2004; Brzinski III et al., 2013; Kang et al., 2018; Feng et al., 2019; Miyai et al., 2019; Roth et al., 2021; Roth, 2021). We define the vertical pressure $P_z \equiv F_z/A$ to account for the cross-sectional area A of the intruder. Accordingly, it is common to characterize the strength of granular materials using a resistance k [N/m^3] parameter determined from:

$$P_z = kh + P_0, \tag{1}$$

where P_0 is the pressure associated with the start of the linear regime. Recent work has shown that the penetration resistance of sand can be understood through a modified Archimedes law, which states that the resisting force is determined by the volume, V, of material being displaced:

$$F_z = K\rho_b g V, \tag{2}$$

where g is gravity, $\rho_b = \phi\rho_p$ is the bulk density of the granular material where ρ_p is particle density and ϕ is the solid volume fraction (one minus porosity), and K is a constitutive property of the material that depends only on the interparticle friction μ (Brzinski III et al., 2013; Roth et al., 2021; Kang et al., 2018). The penetration force response with depth may be composed of three distinct regimes: (i) an initial superlinear regime (not always present (Brzinski III et al., 2013)) associated with material compression beneath the intruder; and (ii) a second sublinear regime, where the fully-formed stagnant cone with volume V_0, determined by the internal friction angle and intruder geometry, begins to displace surrounding material (Feng et al., 2019). With further penetration the displaced volume grows with depth as $V = V_0 + hA$ where the immersed intruder volume is hA (Kang et al., 2018). There is a transition to a (iii) linear regime that occurs when the immersed volume is larger than the stagnant cone; this corresponds generally to a dimensionless depth $\tilde{h} \equiv h/R_e = \tilde{h}_0 < 1$, where $R_e \equiv \sqrt{A/\pi}$ is the equivalent intruder radius. Experiments with varying particle size, shape and volume fraction, and intruder geometry, were collapsed onto a single master curve by nondimensionalizing the penetration resistance, $\tilde{p}_u \equiv P_z/\rho_b g R_e$. Accordingly, for $\tilde{h} > \tilde{h}_0$ the penetration curve can be fit with a dimensionless version of Eq. 1:

$$\tilde{p}_u = K\tilde{h} + \tilde{p}_0, \tag{3}$$

where $\tilde{p}_0$ represents the dimensionless pressure associated with the crossover to the linear regime.

Increasing volume fraction increases the number of particle contacts (Tapia et al., 2013; Aguilar & Goldman, 2016) and hence the effective friction. For a given granular material the range of possible volume fractions is bounded by $\phi_{min} \leq \phi \leq \phi_{max}$, where ϕ_{min} and ϕ_{max} correspond to the loosest and closest packing geometries that can be achieved, respectively. At ϕ_{min}, deformation can occur under any finite stress. As ϕ increases, progressively larger stresses must be applied in order to deform the material; as $\phi \to \phi_{max}$ the yield stress diverges (Nedderman, 1992; Richard et al., 2005; Gravish & Goldman, 2014; Behringer & Chakraborty, 2018). Experiments have shown that increasing ϕ by a factor of ~ 0.1 causes μ to increase by a factor of 20-30 (Horváth et al., 1996; Schröter et al., 2005; Métayer et al., 2009; Furuta et al., 2019). In addition, there is a critical volume fraction ϕ_c associated with complete yielding of granular material: deformation with $\phi < \phi_c$ will lead to compaction, while for $\phi > \phi_c$ the pack must dilate to accommodate deformation (Salgado, 2012; Andreotti et al., 2013; Tapia et al., 2013). For cohesionless, uniform spheres the characteristic values of the important volume fractions are $\phi_{min} \approx 0.56$, $\phi_c \approx 0.59$ and $\phi_{max} \approx 0.64$. These values, however, vary significantly with granular material properties (Cubrinovski & Ishihara, 1999, 2002; Wouterse et al., 2007; Das et al., 2012; Kostynick et al., 2022) and must be determined empirically. We will refer to the packing range $\phi_{max} - \phi_{min}$ as compactibility (Das et al., 2012). Compactibility for natural soils increases nonlinearly with the proportion of fine grains (silt and below) (Cubrinovski & Ishihara, 2002) – due to decreasing ϕ_{min} that results from cohesion holding loose soil together, and increasing ϕ_{max} because of grain-size polydispersity that allows small grains to fill the voids among larger grains (Miura et al., 1997; Cubrinovski & Ishihara, 2002; Dias et al., 2004; Kouraytem et al., 2016; Guida et al., 2020). Data compilations show that soil resistance, measured by the standard penetration test (Rogers, 2006), is inversely related to compactibility; and that compactibility is inversely related to median grain size (Cubrinovski & Ishihara, 1999; Das et al., 2012).

2.2 Experimental setup and laboratory study

The leg we use in this study is a slightly modified version of the device described by (Qian et al., 2019), so we refer to that study for details. The intruder body is a rod with a square cross section that is 1.27 cm wide; tips with various geometries were attached to verify that results were insensitive to tip shape. The rod is pushed downward normal to the surface at a constant speed $v = 1$ cm/s, well within the quasistatic regime (below a grain settling speed, $v_c = \sqrt{2gd} \sim 10$ cm/s, where d is the mean grain diameter) (Roth et al., 2021). At a sampling interval of 0.01 cm, the position of the leg is recorded by the motor encoders while the resisting normal force is measured by converting the estimated motor torque to radial and tangential forces. The rod is pushed to a maximum depth h_{max} of 8 cm.

We validated our penetrometer in the laboratory using quartz sand with diameter $d = 225$ μm placed into a custom air-fluidizing chamber, made of a cylinder of diameter 21.6 cm (Fig. 2b) that is large enough to avoid boundary effects (Seguin et al., 2008; Brzinski III et al., 2013; Kang et al., 2018). The chamber was filled to a depth of 26.7 cm, and an upward flow was applied that was sufficient to completely fluidize the bed. This ensured that the initial state for all experiments was reproducible, as it is known that the strength of granular materials is sensitive to preparation protocol (Krantz, 1991; Albert et al., 1999; Lohermann et al., 2003; Goldman & Umbanhowar, 2008; Montanari et al., 2017). This procedure produced a granular pack with $\phi = 0.57$. From this initial configuration, a weighted plate was placed on the granular surface and it was allowed to slowly compress to achieve a packing fraction of $\phi = 0.59$. We tested a variety of different convex and flat-bottomed intruder tip shapes including triangular, cylindrical, half-

spherical, conical, and cubic (Fig. 2c, inset) for sand with a fixed volume fraction $\phi = 0.57$.

2.3 Field study

Field measurements were collected on September 23, 2020 on a hillslope in Wissahickon Valley Park, located in Philadelphia, PA, USA (Fig. 1a). This location was chosen because it contains many features considered to be representative of the canonical temperate hillslope profile: a ridge of exposed bedrock, a convex profile with increasingly weathered soil moving downslope (Carson & Kirkby, 1972; Selby, 1993), and a fluvial valley bottom (Fig. 1c). We collected data at ∼5 m intervals along two ∼200 m long transects (A and B) from near the ridge to near the valley bottom; both transects had roughly 80 m in elevation change, and followed a path roughly perpendicular to elevation contours. At each site we performed an *in-situ* penetration test with the robotic leg, measured relative soil moisture *in-situ* using a Sinometer VC97 Digital Multimeter, and collected soil samples for grain size analysis using a Beckman-Coulter LS-13-320 Laser Diffraction Particle Size Analyzer. A 60° equilateral triangular tip was used for all field penetration tests, and loose leaf litter and other detritus was gently brushed off of the surface to reach bare soil before the start of penetration (Fig. 1d).

We examined a Digital Elevation Model (DEM) of LiDAR obtained from Pennsylvania Spatial Data Access (PASDA) in QGIS (Fig. 1a). Fifteen elevation profiles were pulled from the DEM, and radially averaged to produce a representative profile of elevation η versus distance x downslope of the origin ($x = 0$) for the hillslope (Fig. 1b). Each downslope location was then projected onto the equivalent downslope location x in the radially-averaged profile, so that we could combine data from both transects to examine downslope trends. We can see that η decreases monotonically with x, and that the morphology exhibits the typical convex hillslope profile.

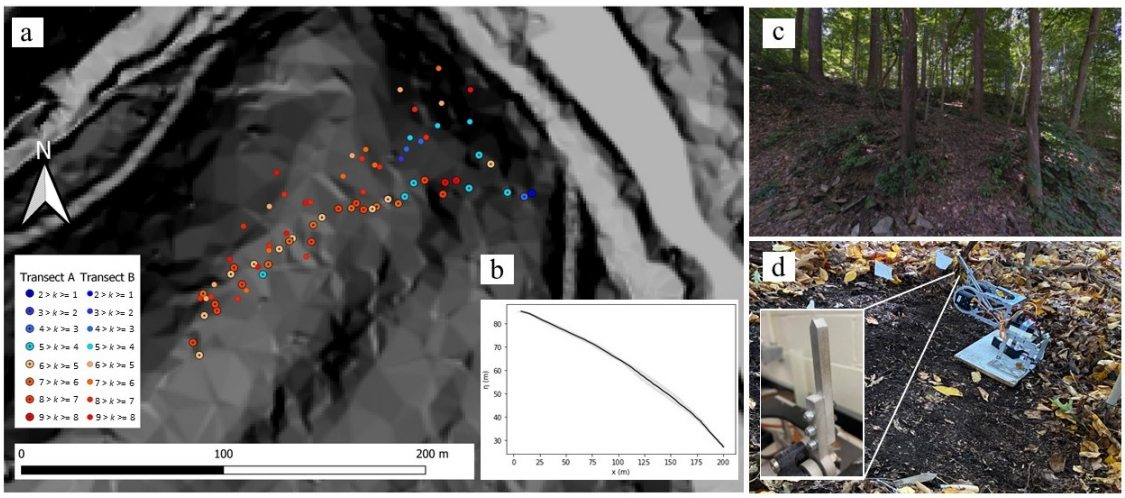

Figure 1: Field setting. (a) Slopeshade image of Wissahickon Valley Park, overlain with locations from each transect, color-coded to reflect penetration resistance k fit from Eq. 1. (b) Mean elevation profile of the hillslope, with the area in gray representing one standard deviation from the mean in both directions. (c) Image facing upslope from the valley of the selected hillslope. (d) Robotic leg prepared for field site measurements. Inset: triangular tip attached to robotic leg for field site measurements.

3 Results

3.1 Laboratory observations

Pressure-depth curves in cohesionless sand exhibit all of the qualitative features reported in previous studies: an initial superlinear increase of P_z with h, followed by a sublinear regime, and a transition to a linear steady-state regime for depths significantly larger than the intruder radius (Fig. 2c, 2d). Results are repeatable (Fig. S3) and insensitive to the intruder tip geometry (Fig. 2c). We examine the influence of changing volume fraction by nondimensionalizing and fitting the third regime of the pressure curves to Eq. 3. This accounts for bulk density differences and allows us to extract K, which should only be a friction parameter. Measurements demonstrate how sensitive granular strength is to changes in volume fraction; the observed reduction in K from $\phi = 0.59$ to $\phi = 0.57$ (Fig. 2d) is comparable to results reported from simulations (Kang et al., 2018) and previous experiments (Horváth et al., 1996; Schröter et al., 2005; Métayer et al., 2009; Furuta et al., 2019).

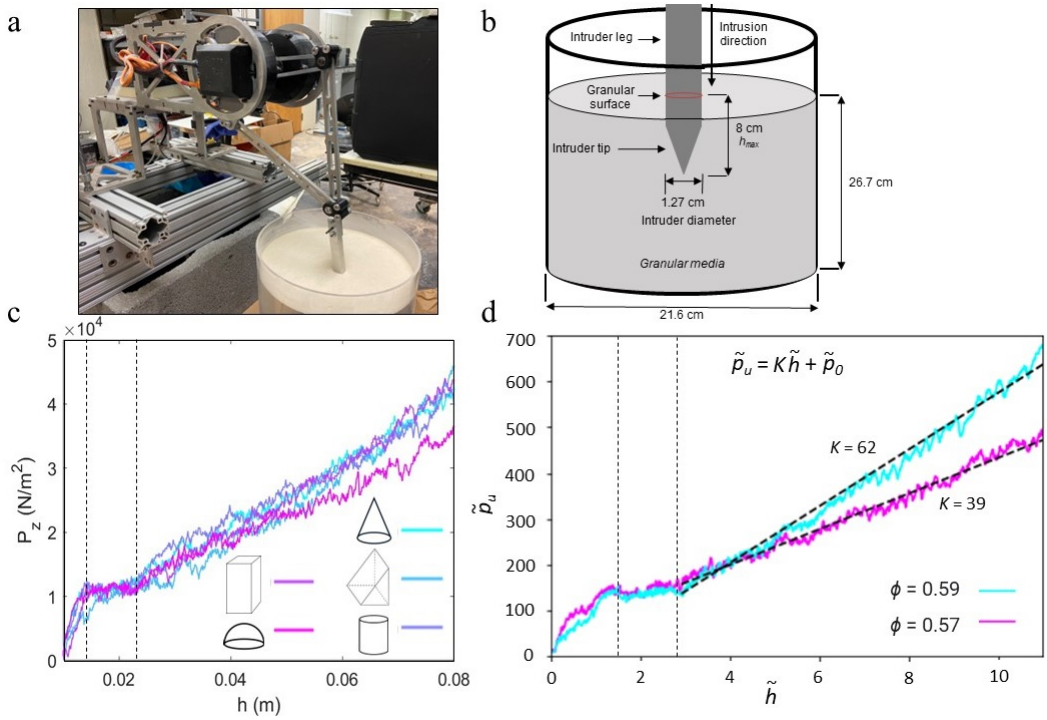

Figure 2: Laboratory penetration tests. (a) Robotic leg during intrusion into air-fluidizing chamber filled with 225 μm sand. (b) Sketch of the experimental apparatus. (c) Averaged normal pressure against intrusion depth; 10 measurements were taken for each tip geometry. Inset: corresponding tip geometries used in experiments. The top of the intruder is oriented in the direction of intrusion. (d) Dimensionless pressure-depth results from laboratory intrusion tests in compacted and loose sand. Dashed lines indicate the linear fit; associated values for K are shown. Dashed vertical lines in (c) and (d) indicate the three identified regimes during intrusion.

3.2 Field observations

We now examine the hillslope profile from Wissahickon Valley Park, starting with soil composition. Soil moisture increased modestly going downslope (Fig. S1a), but this was due primarily to increased water retention by fine grained materials (Fig. S1b). Mois-

ture levels changed only slightly following a rain storm (Fig. S2a), and did not appear to be a dominant factor in soil strength (Fig. S2b; see below), so soil moisture is not considered further. Ridge-top soils appeared to be mostly cohesionless sand with little to no visible clay or organic matter. In contrast, valley bottom soils were dark in color, clearly contained plant litter and other organic material, were dominated by mm-size aggregates that could be balled up in the hand, and had visibly high porosity. Quantitative measurements of particle size distributions support these observations. Ridge-top soils have modes associated with coarse (~ 500 μm) and medium (~ 200 μm) sand, and contain relatively little material below the medium silt (~ 30 μm) range. Although there is significant variation, the general trend moving downslope is that the coarse sand mode decreases in amplitude, while soil becomes progressively enriched in particles below the medium silt range (Fig. 3a). Choosing the median particle diameter d_{50} as representative, we observe a general trend of downslope fining that qualitatively mirrors topography, markedly decreasing around an inflection point in topography; this is in agreement with reported patterns in other temperature hillslopes (Carson & Kirkby, 1972; Yoo et al., 2011)(Fig. 4a).

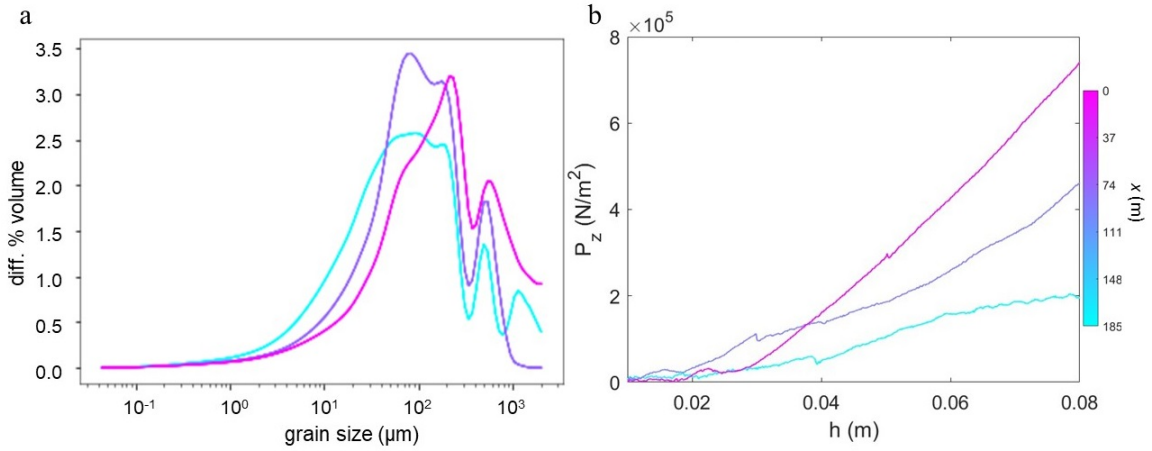

Figure 3: Composition and strength change along a downslope gradient. (a) Soil grain size histogram of select transect A samples, (b) Select normal pressure against intrusion depth curves showing the range of mechanical responses on the hillslope for the locations shown in Fig. 3a. Colorbar corresponds to sample relative downslope distance.

It appears that soil changes from predominantly cohesionless sand with limited compactibility at the ridge ($x = 0$), to cohesive aggregates with relatively low volume fraction and high compactibility at the valley bottom. Granular penetration tests reveal quantitative (Fig. 1a) and qualitative (Fig. 3b) changes in the mechanical properties of soil moving along this gradient. Except for the absence of the initial superlinear regime (i), pressure-depth curves for ridge-top soils exhibit similar behavior to our laboratory measurements of cohesionless sand (Fig. 3b). After an initial sublinear regime (ii), there is a well-developed steady-state regime (iii) where P_z increases linearly with h for soils close to $x = 0$. Pressure values for these sand-rich soils are significantly higher than our laboratory measurements, suggesting that sand-rich field soils are more compacted than the laboratory prepared sand. Moving downslope we observe a general weakening of soil with increasing x, as indicated by the reduced values for P_z at most depths (Fig. 3b, S4). More, we observe that some valley bottom soils do not exhibit a clearly defined linear regime (Fig. 3b, S4). This behavior indicates that finer grained, weathered soils do not behave like a uniform, cohesionless granular material, and that Equations (1) and (3) may not be appropriate. Nevertheless, in order to parameterize soil resistance for comparison across

all samples we force a linear fit of the dimensional Eq. 1 to all P_z-h curves. We use the last 4 cm of the penetration curve for this fit, in order to avoid the (poorly defined) transient regime (ii). Examining data along the hillslope profile, it is clear that soil resistance k is highly variable and that this variability is comparable to any downslope trend (Figs. 1a, 4b). The reproducibility in laboratory measurements (Fig. S3) indicates that the observed variability in field data is not measurement error; results are consistent with our anecdotal experience that soil strength changes in the vicinity of trees and local outcropping of rock. Even so, some general patterns can be observed. First, resistance is more uniform in the upper portion of the hillslope associated with sand rich soils, and becomes significantly more variable around the location $x \approx 125$ m where the d_{50} begins to rapidly decline and soils become more cohesive (Fig. 4). Second, there is an overall trend of decreasing k moving downslope, corresponding to a weakening of soil by a factor of ~ 2 moving from ridge-top to valley bottom (Figs. 1a, 4b).

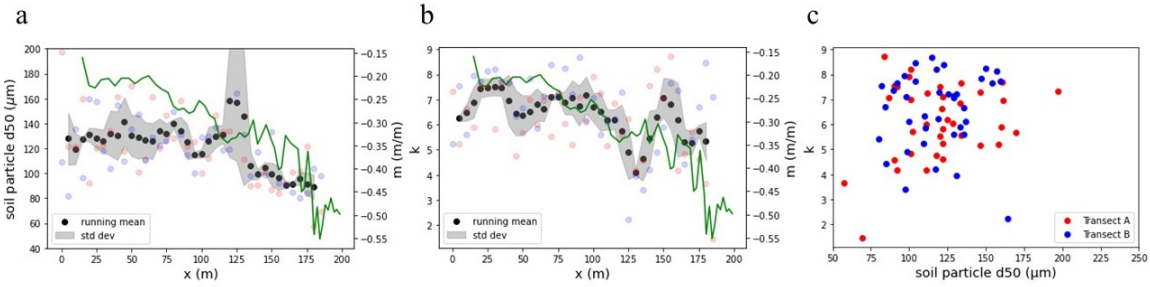

Figure 4: Trends in soil grain size and strength. (a) Soil sample d_{50} against x and slope, m. (b) k against x and slope, m. Black dots are produced from a running mean of soil particle d_{50} and k, each against distance downslope. Area in gray is a standard deviation envelope of the mean soil particle d_{50} and mean k data from both transects. Green line is the central difference slope profile. (c) Relation between k and d_{50} for all data.

Both soil strength and grain size gradually decrease moving from the upslope ridge portion to the downslope valley bottom portion of the hillslope as soil becomes progressively weathered (Fig. 4a, 4b). Resistance is positively correlated, albeit rather loosely, with grain size (Fig. 4c), although it is clear from the scatter in the data that other factors beyond d_{50} control the mechanical strength of soil.

4 Discussion

Progressive weathering of soil from hillslope ridge to valley results in increasing compactibility and a gradual weakening in soil strength. From compilations of soil data provided by (Cubrinovski & Ishihara, 2002), we would expect that our observed reduction in median grain size from $d_{50} \approx 0.13$ mm at $x = 0$ to $d_{50} \approx 0.08$ mm near $x = 200$ m should increase compactibility by a factor of roughly 1.5. Our observed reduction in resistance of roughly a half is consistent with the inferred compactibility change. For granular materials that exhibit a linear mechanical response to normal forcing, k is a measure of resistance directly related to the friction coefficient of the material. For cohesive soils with penetration curves that are sometimes nonlinear, k is still a measure of penetration resistance that is relevant for any intruder – a tree root or burrowing animal, shovel or foot. Resistance, however, results from both friction and cohesion and our test cannot separate these two. It therefore remains useful to compare k across linear and nonlinear soils, but not convert all of these values to friction. The first order pattern is that k gradually decreases downslope, and variability in k increases downslope. Closer examination suggests this hillslope exhibits two regions: an upslope portion of sandy soil

with relatively uniform grain size and strength, and a downslope portion composed of clay-rich soils that are weaker and cohesive. The transition between them occurs in the vicinity of an inflection in the slope profile, likely determined by local geology, where grain size and strength vary the most. Approaching this point at x = 125 m, there are pronounced fluctuations in both soil strength and d_{50}, followed by a decrease in soil strength that coincides with a rapid decrease in d_{50} (Fig. 4a, 4b). The change in soil strength along this gradient is not systematic; variability in k comes from two sources. First, estimates of k for soils in the downslope portion are more error prone, because the penetration curves do not always exhibit a reliably linear regime – likely due to voids, roots and even layering of soil (Fig. 3b). Second, there are true differences in resistance; progressive downslope enrichment in fine particles, due to production of clays by weathering, leads to a systematic increase in soil cohesion. From the perspective of intrusion, cohesion effectively makes soil weaker because it consequently becomes more compactible. This may be one difference from what would occur under fluid shear flow (Dunne & Jerolmack, 2020).

Geotechnical equipment developed for probing deep soil profiles is not adequately sensitive for studying shallow (up to ~ 0.1 m) soil behavior. Downslope soil transport in temperate hillslopes like the Wissahickon are not shaped primarily by overland or shear flow processes, but rather by creep. The soil strength that we probe is relevant for understanding biophysical disturbance from intruders – roots, burrowing animals and foot traffic – which may deform and destabilize soil. A soil's response to an intruder remains normal to the intruder tip, even when penetrated at an angle; there are little to no shear forces during these interactions (Brzinski III et al., 2013). In other words, vertical penetration tests are effective for measuring friction and resistance for most intruder-ground interactions. The granular penetrometer used here resolves these shallow depths, and provides field measurements that are comparable in quality to laboratory experiments. The time efficiency of our penetration test allows one to map soil strength across an entire landform under approximately constant environmental conditions (Fig. 1a). The heterogeneity observed on the studied hillslope demonstrates the importance of gathering a large dataset, in order to reveal underlying patterns like the downslope gradient in k that we observe. Our penetrometer can be attached to a proproceptive legged robot (Kenneally & Koditschek, 2016) for automated mapping of soil strength across landscapes, which offers advantages over wheels in navigating steep terrain and loose soil (Zhang et al., 2013; Roberts, Duperret, Li, et al., 2014; Roberts, Duperret, Johnson, et al., 2014; Kenneally & Koditschek, 2016; Qian et al., 2015, 2017; Kolvenbach et al., 2022). This is useful for hazard avoidance by detecting dangerously loose soil, with further potential for exploring planetary surfaces such as the Moon and Mars. The failure of the Martian geothermal probe informally called "the mole" became an accidental experiment in granular penetration (Spohn et al., 2022) — and a cautionary tale about the hazards of predicting granular behavior in unknown environments.

5 Open Research

Data and source code associated with this manuscript is available on GitHub (`https://github.com/johnruck-sed/GRL_2023_RobotRheometer`). Data is permanently deposited in Zenodo (Ruck, 2023). Data used in the development of the digital elevation model (`https://www.pasda.psu.edu/download/pamap/pamap_lidar/cycle1/DEM/South/2008/20000000/27002680PAS_dem.zip`) is publicly available and was downloaded from PASDA using the Pennsylvania Imagery Navigator (`https://maps.psiee.psu.edu/ImageryNavigator/`).

6 Acknowledgments

We acknowledge funding from NSF-MRSEC (NSF-DMR-1720530), NSF-NRI (NSF-NRI-INT-1734355), and NASA-PSTAR (80NSSC22K1313). We thank Shravan Pradeep,

Sophie Silver, Chen Li, and Eric Sigg for helpful discussions. Authors have no conflict of interest to declare.

References

Aguilar, J., & Goldman, D. (2016). Robophysical study of jumping dynamics on granular media. *Nature Phys*, *12*, 278–283.

Albert, R., Pfeifer, M., Barabá si, A., & Schiffer, P. (1999). Slow drag in a granular medium. *Physical Review Letters*, *82*(1), 205.

Andreotti, B., Forterre, Y., & Pouliquen, O. (2013). *Granular media between fluid and solid*. Cambridge University Press.

Ballantyne, C. (2009). Earth surface processes, landforms and sediment deposits. *Journal of Quaternary Science*, *24*(6), 642-642.

Behringer, R., & Chakraborty, B. (2018). The physics of jamming for granular materials: a review. *Reports on Progress in Physics*, *82*(1).

Briaud, J. (2013). *Geotechnical engineering: Unsaturated and saturated soils*. Hoboken, New Jersey: John Wiley & Sons, Inc.

Briaud, J.-L., Shafii, I., Chen, H.-C., & Medina-Cetina, Z. (2019). *Relationship between erodibility and properties of soils*. National Cooperative Highway Research Program, The National Academies Press.

Bronick, C., & Lal, R. (2005). Soil structure and management: a review. *Geoderma*, *124*(1), 3–22.

Bryan, R. B. (2000). Soil erodibility and processes of water erosion on hillslope. *Geomorphology*, *32*(3-4), 385–415.

Brzinski III, T., Mayor, P., & Durian, D. (2013). Depth-dependent resistance of granular media to vertical penetration. *Physical Review Letters*, *111*(16).

Carson, M., & Kirkby, M. (1972). *Hillslope form and process*. Cambridge University Press.

Chhaniyara, S., Brunskill, C., Yeomans, B., Matthews, M., Saaj, C., Ransom, S., & Richter, L. (2012). Terrain trafficability analysis and soil mechanical property identification for planetary rovers: A survey. *Journal of Terramechanics*, *49*(2).

Cubrinovski, M., & Ishihara, K. (1999). Empirical correlation between spt n-value and relative density for sandy soils. *Soils and Foundations*, *39*(5), 61–71.

Cubrinovski, M., & Ishihara, K. (2002). Maximum and minimum void ratio characteristics of sands. *Soils and foundations*, *42*(6), 65–78.

Das, B., Sivakugan, N., & Atalar, C. (2012). Maximum and minimum void ratios and median grain size of granular soils: their importance and correlations with material properties. In *Proceeding of* (Vol. 3).

Dias, R., Teixeira, J., Mota, M., & Yelshin, A. (2004). Particulate binary mixtures: dependence of packing porosity on particle size ratio. *Ind. Eng. Chem. Res.*, *43*(24), 7912–7919.

Diel, J., Vogel, H.-J., & Schlüter, S. (2019). Impact of wetting and drying cycles on soil structure dynamics. *Geoderma*, *345*, 63–71.

Dunne, K., & Jerolmack, D. (2020). What sets river width? *Science Advances*, *6*(41). doi: 10.1126/sciadv.abc1505

Famiglietti, J., Rudnicki, J., & Rodell, M. (1998). Variability in surface moisture content along a hillslope transect: Rattlesnake hill, texas. *Journal of Hydrology*, *210*(1), 259–281.

Feng, Y., Blumenfeld, R., & Liu, C. (2019). Support of modified archimedes' law theory in granular media. *Soft Matter*, *15*(14).

Furuta, T., Kumar, S., Reddy, K., Niiya, H., & Katsuragi, H. (2019). Packing-dependent granular friction exerted on a rod withdrawn from a granular layer: the role of shear jamming. *New Journal of Physics*, *21*, 023001.

Goldman, D., & Umbanhowar, P. (2008). Scaling and dynamics of sphere and disk impact into granular media. *Physical Review E*, *77*(2).

Gravish, N., & Goldman, D. (2014). Effect of volume fraction on granular avalanche dynamics. *Physical Review E*, *90*(3).

Guida, G., Einav, I., Marks, B., & Casini, F. (2020). Linking micro grainsize polydispersity to macro porosity. *International Journal of Solids and Structures*, *187*, 75–84.

Hawley, M., Jackson, T., & McCuen, R. (1983). Surface soil moisture variation on small agricultural watersheds. *Journal of Hydrology*, *62*(1-4), 179–200.

Horváth, V., Jánosi, I., & Vella, P. (1996). Anomalous density dependence of static friction in sand. *Physical Review E*, *54*(2).

Huggett, R. (2011). *Fundamentals of geomorphology (3rd ed.)*. Routledge.

Janda, A., & Ooi, J. (2016). Dem modeling of cone penetration and unconfined compression in cohesive solids. *Powder Technology*, *293*, 60–68.

Just, G., Smith, K., Joy, K., & Roy, M. (2020). Parametric review of existing regolith excavation techniques for lunar in situ resource utilisation (isru) and recommendations for future excavation experiments. *Planetary and Space Science*, *180*.

Kang, W., Feng, Y., Liu, C., & Blumenfeld, R. (2018). Archimedes' law explains penetration of solids into granular media. *Nature Communications*, *9*(1101).

Kenneally, G., & Koditschek, D. (2016). Design principles for a family of direct-drive legged robots. *IEEE Robotics and Automation Letters*, *1*(2), 900–907.

Kolvenbach, H., Arm, P., Hampp, E., Dietsche, A., Bickel, V., Sun, B., ... Hutter, M. (2022). Traversing steep and granular martian analog slopes with a dynamic quadrupedal robot. *Field Robotics*, *2*, 910 – 939.

Kostynick, R., Matinpour, H., Pradeep, S., Haber, S., Sauret, A., Meiburg, E., ... Jerolmack, D. (2022). Rheology of debris flow materials is controlled by the distance from jamming. *Proc Natl Acad Sci USA*, *119*(44).

Kouraytem, N., Thoroddsen, S., & Marston, J. (2016). Penetration in bimodal, polydisperse granular material. *Physical Review E*, *94*(5), 052902.

Krantz, R. (1991). Measurements of friction coefficients and cohesion for faulting and fault reactivation in laboratory models using sand and sand mixture. *Tectonophysics*, *188*.

Lohermann, J., Kukowski, N., Adam, J., & Onken, O. (2003). The impact of analogue material properties on the geometry, kinematics, and dynamics of convergent sand wedges. *Journal of Structural Geology*, *25*.

Mayne, P., & Dumas, C. (1997). Enhanced in situ geotechnical testing for bridge foundation analysis. *Transportation Research Record*, *1569*(1).

Miura, K., Maeda, K., Furukawa, M., & Toki, S. (1997). Physical characteristics of sands with different primary properties. *Soils and Foundations*, *37*(3), 53–64.

Miyai, S., Kobayakawa, M., Tsuji, T., & Tanaka, T. (2019). Influence of particle size on vertical plate penetration into dense cohesionless granular materials (large-scale dem simulation using real particle size). *Granular Matter*, *21*(105), 1580-1587.

Montanari, D., Agostini, A., Bonini, M., Corti, G., & Ventisette, C. (2017). The use of empirical methods for testing granular materials in analogue modelling. *Materials (Basel)*, *9*(10).

Métayer, J.-F., Delannay, R., Richard, P., Valance, A., & Louge, M. (2009). Rheology of confined granular flows: from gas to glass. *AIP Conference Proceedings*, *1145*(1), 503–506.

Nedderman, R. (1992). *Statics and kinematics of granular materials.* Cambridge University Press.

Paaswell, R. (1973). Causes and mechanisms of cohesive soil erosion: The state of the art. *Soil Erosion: Causes and Mechanisms: Prevention and Control,*

Conference Workshop on Soil Erosion, Highway Research Board Special Report(135).

Qian, F., Jerolmack, D., Lancaster, N., Nikolich, G., Reverdy, P., Roberts, S., ... Koditschek, D. (2017). Ground robotic measurement of aeolian processes. *Aeolian Research*, *27*, 1-11.

Qian, F., Lee, D., Nikolich, G., Koditschek, D., & Jerolmack, D. (2019). Rapid in situ characterization of soil erodibility with a field deployable robot. *Journal of Geophysical Research: Earth Surface*, *124*, 1261–1280.

Qian, F., Zhang, T., Korff, W., Umbanhowar, P., Full, R., & Goldman, D. (2015). Principles of appendage design in robots and animals determining terradynamic performance on flowable ground. *Bioinspiration Biomimetics*, *10*, 056014.

Richard, P., Nicodemi, M., Delannay, R., Ribiére, P., & Bideau, D. (2005). Slow relaxation and compaction of granular systems. *Nature Materials*, *4*, 121–128.

Richefeu, V., Said El Youssoufi, M., & Radjai, F. (2006). Shear strength properties of wet granular materials. *Physics Review E*, *73*(5).

Roberts, S., Duperret, J., Johnson, A., Van Pelt, R., Zobeck, T., Lancaster, N., & Koditschek, D. (2014, 11). Desert rhex technical report: Jornada and white sands trip.

Roberts, S., Duperret, J., Li, X., Wang, H., & Koditschek, D. (2014). *Desert rhex technical report: Tengger desert trip* (Tech. Rep.). ESE.

Rogers, J. (2006). Subsurface exploration using the standard penetration test and the cone penetrometer test. *Environmental Engineering Geoscience*, *12*(2), 161–179.

Roth, L. (2021). Constant speed penetration into granular materials: drag forces from the quasistatic to inertial regime. *Granular Matter*, *23*(3), 54.

Roth, L., Han, E., & Jaeger, H. (2021). Intrusion into granular media beyond the quasistatic regime. *Physics Review Letters*, *126*(21).

Ruck, J. (2023). *johnruck-sed/GRL_2023_RobotRheometer:open_research.* [Software]. Zenodo. Retrieved from `https://doi.org/10.5281/zenodo.8370598`

Salgado, R. (2012). The mechanics of cone penetration: Contributions from experimental and theoretical studies. *Geotechnical and Geophysical Characterization*, *4*, 131–135.

Santamarina, J., & Cho, G. (2004). Soil behaviour: The role of particle shape. *The Skempton Conferences*.

Saravanan, R., Poongodi, K., Murthi, P., Sudharshan, E., & Gobinath, R. (2020). Effect of particle grain size on its shear strength behaviour of soils. *IOP Conf. Ser.: Mater. Sci. Eng.*, *981*(032079).

Schröter, M., Goldman, D., & Swinney, H. (2005). Stationary state volume fluctuations in a granular medium. *Phys Rev E Stat Nonlin Soft Matter Phys*, *71*, 030301.

Seguin, A., Seguin, B., Philippe, Y., & Philippe, G. (2008). Influence of confinement on granular penetration by impact. *Physics Review E*, *78*(1).

Selby, M. (1993). *Hillslope materials and processes.* Oxford University Press.

Seweryn, K., Skocki, K., Banaszkiewicz, M., Grygorczuk, J., Kolano, M., Kuciński, T., ... Wawrzaszek, R. (2014). Determining the geotechnical properties of planetary regolith using low velocity penetrometers. *Planetary and Space Science*, *99*.

Spohn, T., Hudson, T., Witte, L., Wippermann, T., Wisniewski, L., Kedziora, B., ... Grygorczuk, J. (2022). The insight-hp3 mole on mars: Lessons learned from attempts to penetrate to depth in the martian soil. *Advances in Space Research*, *69*(8), 3140–3163.

Stone, M., Barry, R., Bernstein, D., Pelc, M., Tsui, Y., & Schiffer, P. (2004). Local jamming via penetration of a granular medium. *Phys. Rev. E*, *70*(4).

Tapia, F., Espíndola, D., Hamm, E., & Melo, F. (2013). Effect of packing fraction on

shear band formation in a granular material forced by a penetrometer. *Phys. Rev. E*, *87*.

Vu, E., Schaumann, G., & Buchmann, C. (2022). The contribution of microbial activity to soil–water interactions and soil microstructural stability of a silty loam soil under moisture dynamics. *Geoderma*, *417*, 115822.

Wouterse, A., Williams, S., & Philipse, A. (2007). Effect of particle shape on the density and microstructure of random packings. *Journal of Physics: Condensed Matter*, *19*(40).

Wroth, C. (1984). The interpretation of in situ soil tests. *Geotechnique*, *34*(4), 449–489.

Yoo, K., Weinman, B., Mudd, S., Hurst, M., Attal, M., & Maher, K. (2011). Evolution of hillslope soils: The geomorphic theater and the geochemical play. *Applied Geochemistry*, *26*, S149-S153.

Zhang, T., Qian, F., Li, C., Masarati, P., Hoover, A., Birkmeyer, P., ... Goldman, D. (2013, 06). Ground fluidization promotes rapid running of a lightweight robot. *The International Journal of Robotics Research*, *32*, 859-869. doi: 10.1177/0278364913481690